Magnetic Equivalent Circuit Method for Analysis of PM Flux Distribution in Axial Flux Permanent Magnet Consequent Pole Generator

Mahmoud Marousi Noushabadi[1], Saeid Javadi*[2] & Samad Taghipour Boroujeni[3]

[1] Department of Electrical and Computer Engineering, Kashan Branch, Islamic Azad University, Kashan, Iran

[2] Department of Electrical and Computer Engineering, Kashan Branch, Islamic Azad University, Kashan, Iran

[3]Engeeniering and Technology Department, Shahrekord University, Shahrekord, Iran

Abstract

According to the advantages of consequent pole machines, this paper presents a fast analytical model for estimating the components of the PM flux density distribution in the air gap for an axial flux permanent magnet consequent pole generator (AFPM-CP). The sample generator has a double-sided structure with a sector coil and poles. N identical poles (with only identical N poles in sequence and iron poles between them) are installed on the rotor, and the stator is placed between the rotors. The stator consists of coils that are wrapped concentrically around the teeth. A one-dimensional analytical solution based on the magnetic equivalent circuit method and a two-dimensional analytical solution based on the finite element method were presented to predict the performance characteristics of a three-phase AFPM-CP under no-load operating conditions. The effects of the stator slots have been studied using the air gap and flux path function methods. For verification purposes, the magnetic equivalent circuit (MEC) analytical results are compared with those of the finite element method (FEM). To further validate the MEC analytical and FEM results, 3D-FEM analysis has also been performed. This means that the proposed MEC method is effective for the AFPM-CP machine.

Keywords: Equivalent Circuit Method, Finite Element Method, Axial Flux Machine, Permanent Magnet, Consequent pole, Generator

1-Introduction

Axial flux permanent magnet machines are attractive for applications such as electric vehicles, marine industries, aerospace industries, energy storage devices, power generation, and other industrial applications [1,2,3]. These machines are a convincing alternative to conventional radial flux machines due to their features such as compact structure, short axial length relative to the outer diameter, lightweight, large power/torque density, low losses, high efficiency, the ability to integrate quickly and easily with other mechanical equipment and the possibility of increasing the number of poles [4,5,6,7]. Axial flux permanent magnet machines have different types of structures based on the placement of magnets, slots, cores, coils, and multi-stage. These machines can generally be classified into three categories: single-sided, double-sided, and multi-stage [8].

Single-sided machines consist of one rotor and one stator; the force of attraction between the rotor and the stator in these machines causes unbalance. Multi-stage machines consist of several rotors and stators that are placed in a row, which increases the axial length of the machine. Changing the number of rotors and stators makes it possible to change the torque based on the axial length [9]. Double-sided machines are divided into two categories: Axial flux internal rotor (AFIR) and Axial flux internal stator (AFIS). Both categories are superior in terms of production to single-sided and multi-stage machines because, on the one hand, almost no axial magnetic attraction occurs and, on the other hand, they have a simpler structure than multi-stage machines [10,11,12].

The double rotor structure will be a solution to overcome the axial magnetic attraction force because the net axial force on the rotor is about zero. In addition, it leads to achieving higher power density [13]. In the AFIS structure, the stator is placed in the center, and the permanent magnet rotors are on its sides, which results in fewer end windings in the stator. This reduction significantly improves the machine's efficiency [14].

The axial flux permanent magnet consequent pole machine has several advantages, such as reducing the consumption of rare-earth permanent magnets, minimizing environmental hazards, lowering material and manufacturing costs while maintaining better performance, and featuring a simple and robust structure. It also has a simple rotor construction, simple winding, very low cogging torque, and favorable electrical characteristics. Additionally, it has lower losses and higher efficiency, making it possible to achieve an efficient and economical machine [15,16].

With the introduction of various structures of electrical machines and the need to study them in detail, analytical methods have received more attention. By using analytical methods in the design and modeling of electric machines, it is possible to explore the structure of electrical machines in greater detail. Analytical methods can accurately show the effect of different parameters on the performance of an electric machine [17,18].

Most analytical methods are based on solving one-dimensional (1D) or two-dimensional (2D) equations. Among the one-dimensional (1D) analysis techniques, the MEC and winding function (WF) methods are more common. MEC and WF are widely used to calculate the no-load operation and armature reaction, respectively [17]. However, the accuracy of the MEC and WF methods is reduced in the magnetic flux calculation along the irregular flux path [19].

The 2D analytical solution of the Maxwell equations results in higher accuracy in predicting electromagnetic quantities. For instance, the cogging torque can be calculated by the net lateral force (NLF) method or the Maxwell stress tensor; however, the Maxwell stress tensor has higher accuracy compared to NLF, and Maxwell stress tensor techniques are based on 1D and 2D models, respectively [20]. Some of the well-known 2D analytical techniques are sub-domain (SD) [21,22,23], conformal mapping (CM) [17,24], and virtual surface currents (VSCs) [18,21,25], which are used to compute the air-gap magnetic flux density in electric machines with slotted stator/rotor structures.

Reference [26] proposes an analytical model (AM) for predicting air-gap magnetic flux density in an axial flux permanent magnet machine with a yokeless and segmented armature under the stator module misalignment fault. The finite element method for AFPM machines causes a large computational burden during simulation. Thus, Reference [27] proposes an improved magnetic equivalent circuit method to predict the performance of segmented-Halbach AFPM machines, which can consider the different magnetization directions of Halbach PMs.

The air-gap and tooth-tip leakage flux of AFPM machines with different slots and poles have been analyzed and researched. Firstly, the air-gap leakage coefficient is derived based on the equivalent magnetic circuit model with different slot and pole combinations. Then, the tooth-tip leakage coefficient is calculated using the analytical method and compared with the finite element method [28].

Although the high accuracy of the 3D analytical method is considered an advantage over other analytical methods, the need for extensive analysis time and software skills to use this method is one of its disadvantages. In contrast, analytical methods are very fast and do not depend on software skills.

In this article, a three-phase axial flux permanent magnet generator with a consequent pole structure (AFPM-CP) is analyzed using one-dimensional and two-dimensional analysis methods, with magnetic equivalent circuit methods and finite element analysis methods, respectively. The 3D-FEM analysis has also been used for further validation and comparison of the results

2- Introduction of the analyzed generator

The schematic structure of the proposed axial flux permanent magnet generator with a consequent pole is shown in Figure 1. It consists of a double-sided structure with two rotors and one stator. This model has a simple structure for manufacturing and also reduces the consumption of magnets, which lowers production costs. A tooth-wound winding is wrapped around the iron teeth of the stator and is placed between the two rotors with an air gap of 1 mm. The iron used for the teeth and the rotor has a relative permeability of 4,000 and a bulk conductivity of 10,300,000 Siemens/m.

Sector-shaped magnetic poles made of Nd-Fe-B magnets are placed on the disc-shaped rotor, and instead of using magnetic S poles, iron poles (of the same type as the rotor) are used. The dimensions of the N and S poles are equal. Figure 2 shows the arrangement of machine components from the top view. In this machine, the rotors rotate while the stator remains stationary. If Figure 2 includes the top layer, it cannot show the internal elements like teeth and windings. To address this, we hide the top layer to make all objects visible. Figure 3 illustrates the configuration of machine poles and flux paths in the proposed generator. The primary flux path is represented by solid red lines, while the leakage flux paths are denoted by dashed red lines.

The voltage of each phase of the generator is obtained from the sum of the voltages of two sets of 60-turn concentrated coils connected in series, as shown in Figure 4. Eight types of NdFe35 permanent magnets have been used as magnetic poles. Figure 5 illustrates the schematic of the analytical model with a linear structure, where the sector poles are represented as rectangles. The sector-shaped poles are arranged in an N-iron structure. The general specifications of the AFPM-CP generator are listed in Table 1.

3- Magnetic equivalent circuit analysis method

The 2-dimensional structure of the axial flux permanent magnet consequent pole slotted and slot-less generator at a radius of 30 mm is shown in Figures 6 and 7, respectively. The process begins by analyzing the flow of magnetic flux within the generator, which can be divided into distinct paths, such as through the rotor, stator, and air gap. In the MEC, each of these paths is represented by a reluctance element. The rotor reluctance accounts for the resistance to the flow of magnetic flux in the rotor material, while the stator reluctance corresponds to the flux resistance in the stator material. The air gap reluctance represents the resistance in the air gap, where the magnetic flux passes between the rotor and stator. Additionally, the leakage reluctance model accounts for the flux that does not contribute to useful work but instead leaks across the poles.

The magnetic flux in the system follows a path from the magnets to the rotor, through the stator and air gap, completing the circuit. The reluctances are then combined into an equivalent circuit, where the flux is distributed according to the reluctance of each path. Figure 8 shows the main magnetic equivalent circuit of the slot-less structure, while Figure 9 provides a simplified version of this MEC for easier understanding. With the assumption of linear magnetic behavior and by neglecting saturation effects, the magnetic flux value is determined using Equation (1).

$$\varphi_g = \varphi_r \frac{1}{1+\frac{R_g+\left(\frac{R_r+R_s}{4}\right)}{R_m}+\frac{(8R_g+R_s)(1+\frac{R_r}{4R_m})}{R_l}} \qquad (1)$$

In this equation, R_r, R_s, R_m, R_g , and R_l represent the rotor iron reluctance, stator reluctance, internal reluctance of the magnet, air gap reluctance, and leakage path reluctance between the two poles, respectively. The effect of leakage reluctance can be accounted for using a coefficient, allowing the magnetic air gap flux equation to be simplified, as shown in Equation (2). In this case, the equivalent circuit structure without leakage reluctance is illustrated in Figure 10.

$$\varphi_g = \frac{\frac{\varphi_r}{k_1}}{1+\frac{2R_g+\left(\frac{R_r+R_s}{4}\right)}{R_m}} \qquad (2)$$

The coefficient k_1 value is defined in equation (3). If we assume the relative permeability of the stator and rotor iron to be infinite, the equivalent circuit will be as shown in Figure 11, and the flux value will be obtained as in equation (4). Additionally, the air gap flux density is determined using Equation (5).

$$k_1 = 1-\frac{1}{k\left[\frac{r_r}{B_p(l_g+l_m)}\right]^n+1} \qquad (3)$$

$$\begin{aligned}
\varphi_g &= k_1\varphi_r \frac{1}{1+\frac{2R_g}{R_m}} \\
R_g &\approx \frac{l_g}{\mu_0 A_g} \\
R_m &\approx \frac{l_m}{\mu_0 \mu_r A_m} \qquad (4) \\
\varphi_g &= \varphi_r \frac{K_1}{1+\frac{A_m l_g}{\frac{A_g l_m}{\mu_r}}}
\end{aligned}$$

$$B_g = \frac{\varphi_g}{A_g}, B_{rem} = \frac{\varphi_r}{A_m}$$

$$B_g = B_{rem} \frac{k_1}{\frac{A_g}{A_m} + \frac{2\mu_r l_g}{l_m}} \qquad (5)$$

$$A_g = \frac{A_m l_g \mu_r}{l_m \frac{\varphi_r k_1}{\varphi_g} - 1}$$

In the above equations, r_r, B_p, n, k, A_m, and A_g represent the rotor radius, pole flux density, number of machine layers, leakage correction factor, average magnet area, and air gap of a pole, respectively. Additionally, l_m and l_g denote the magnet thickness and the length of the air gap along the tangent line, respectively. In the above equations, μ_r is the magnetic permeability coefficient, which is almost equal to one.

4- Analysis with considering slot effect

The length of the air gap in slot-less machines is constant, but in slotted stator machines, the main part of the flux tends to pass through the teeth of the stator, while a small part of the flux enters the open area of the stator teeth. There are different methods to consider the stator slot effect, such as the permeability function [29], the air gap function [30], and the flux path function [20], with similar underlying principles. In the air gap function method, the air gap is defined as a function. The value of the function under the stator slot is equal to the height of the slot opening. In addition, the height of the air gap is $(h_{so} + l_{g0})$, and under the tooth, it is equal to the height of the air gap (l_{g0}). Figure 12 shows the flux passing path in the air gap function method.

In reality, the flux density lines' path, which is considered in the flux path function method, is shown in Figure 13. Roughly, it can be said that the flux density lines in the open area of the stator slot travel a length equal to a quarter of a circle. The air gap flux density equation (4) is zero-dimensional, and the MEC method is also a zero-dimensional analytical method. If we consider the flux density distribution in the air gap according to the arrangement, as shown in Equation (6), the air gap flux density diagram in the vertical direction in terms of θt is obtained.

$$B_r^{ag}(\theta, \theta_r) = \sum_{n=1,3,\ldots}^{\infty} \frac{4B_g}{n\pi} \sin(\frac{n\pi\alpha}{2}) \cos(n\pi(\theta - \theta_r)) \qquad (6)$$

in Equation (6), θ_r represents the rotor position, and α is the relative length of the magnet arc, which is considered equal to 0.955 in this paper. Also, the air gap function under the teeth and the slot is given in Equations (7) and (8), respectively.

$$l_g(\theta) = l_g \qquad (7)$$

$$l_g(\theta) = l_g + h_s \qquad (8)$$

In the above equations, l_g is the height of the air gap, and h_s is the height of the opening of the slot. Using an analytical method, Figure 14 shows the slot-less machine's vertical flux density diagram in the air gap. The length of the air gap in Equation (5) is considered to be 1mm. To validate the results, the analysis has also been performed using a 2-D and 3-D method. As seen in Figure 15, the red line represents the 3-D finite element analysis, the blue line represents the 2-D finite element analysis, and the black line represents the magnetic equivalent circuit analysis. It can be observed that the results of the three methods overlap very well.

Due to the large size of the stator slots, we have considered their effect as a combination of both air gap function and flux path function methods. The flux path and the air gap length are shown in Figures 16 and 17, respectively. If the flux density in terms of θ is obtained from Equation (6), and the air gap is defined as a function, then using an analytical method, the air gap flux density diagram in the vertical direction, considering the slot effect, is obtained in Figure 18.

To validate the results, the analysis has also been performed using 2-D and 3-D method. As seen in Figure 19, the red line represents the 3-D finite element analysis, the blue line represents the 2-D finite element analysis, and the black line represents the magnetic equivalent circuit analysis. It can be observed that the results of the three methods overlap very well.

4-Conclusion

Due to the numerous advantages of consequent pole machines—such as reduced consumption of rare-earth permanent magnets, lower environmental hazards, decreased material and manufacturing costs, improved performance, simple and robust structure, simple rotor construction, simple winding, very low cogging torque, favorable electrical characteristics, lower losses, and higher efficiency—this article investigates and analyzes a sample of an axial flux generator with a consequent pole structure.

A 1-D analytical solution based on the MEC method and a 2-D analytical solution based on the FEM method were presented to predict the performance characteristics of a three-phase axial flux permanent magnet consequent poles generator at no-load operating conditions. The 3D-FEM analysis has also been used for further validation. The generator analysis is performed in two modes: slotted and slotless. In the slot mood, due to the large size of the stator slots, their effect has been considered as a combination of both the air gap function and flux path function methods. In the slotless mood, the length of the air gap is considered equal to 1 mm. By comparing the results, we can see that adding a tooth to the machine increases the flux linkage and, as a result, improves the efficiency of the machine. As is known, the proposed method has high accuracy, is faster than numerical methods based on iteration, and is effective for the AFPM-CP machine.

5-Reference

[1] Nishanth, G., Verdeghem, J.V., and Severson, E.L. “A review of axial flux permanent magnet machine technology”, in IEEE Transactions on Industry Applications., **59**(4), pp. 3920-3933, DOI: 10.1109/TIA.2023.3258933, July-Aug (2023).

[2] Zhuo, H., Ma, Y., et al. “A review of axial-flux permanent-magnet motors: topological structures, design, optimization and control techniques”, Machines **10,12** (1178), https://doi.org/10.3390/machines10121178, (2022).

[3] Yi, F., Zhang,C., et al. “Quasi-3-D analytical method of open-circuit magnetic field for yokeless and segmented armature machine”, in IEEE Transactions on Magnetics, **59**(12), pp. 1-10, Art no. 8104310, DOI: 10.1109/TMAG.2023.3305017, Des (2024).

[4] Kumar, s., Lipo, T.A., and Kwon, B. “A 32 000 r/min axial flux permanent magnet machine for energy storage with mechanical stress analysis”, in IEEE Transactions on Magnetics., **52**(7), pp. 1-4, DOI: 10.1109/TMAG.2015.2512939, July (2016).

[5] Taqavi, O., Abdollahi, SE., and Aslani, B. “Investigations of magnet shape impacts on coreless axial-flux PM machine performances”, 12th Power Electronics, Drive Systems, and Technologies Conference (PEDSTC), pp. 1-5, DOI: 10.1109/PEDSTC52094.2021.9405833, Tabriz, Iran (2021).

[6] Zhao, J., Quan, X., Sun, X., et al. “Design of a novel axial flux rotor consequent-pole permanent magnet machine”, in IEEE Transactions on Applied Superconductivity, **30**(4), pp. 1-6, DOI: 10.1109/TASC.2020.2986743, June (2020).

[7] Patterson, D.J., Colton, J.L., Mularcik, B., et al. “A comparison of radial and axial flux structures in electrical machines”, 2009 IEEE International Electric Machines and Drives Conference, pp. 1029-1035, DOI: 10.1109/IEMDC.2009.5075331, USA (2009).

[8] Kahourzade, S., Mahmoudi, A., Ping, HW., et al. “A comprehensive review of axial-flux permanent-magnet machines", in Canadian Journal of Electrical and Computer Engineering, **37**(1), pp. 19-33, DOI: 10.1109/CJECE.2014.2309322, winter (2014).

[9] Aydin, M., and Gulec, M. “Reduction of cogging torque in double-rotor axial-flux pm disk motors: A review of cost-effective magnet-skewing techniques with experimental verification”, IEEE Transactions on Industrial Electronics, **61**(9), pp. 5025–5034, DOI: 10.1109/TIE.2013.2276777

, (2014).

[10] Lehr, M., Woog, D., and Binder, A. “Design, construction and measurements of a permanent magnet axial flux machine”, 2016 XXII International Conference on Electrical Machines (ICEM), pp. 1604-1610, DOI: 10.1109/ICELMACH.2016.7732738, Lausanne, Switzerland (2016).

[11] Aydin, M., Huang, S., and Lipo, T.A. “Torque quality and comparison of internal and external rotor axial flux surface-magnet disc machines”, in IEEE Transactions on Industrial Electronics, **53**(3), pp. 822-830, DOI: 10.1109/TIE.2006.874268, June (2006).

[12] Lehr, M., Reis, K., and Binder, A. “Comparison of axial flux and radial flux machines for the use in wheel hub drives”, e+i Elektrotechnik und Informationstechnik, **132**, pp. 25–32, https://doi.org/10.1007/s00502-014-0272-3, (2015).

[13] Nobahari, A., Darabi, A., and Hassannia, A. “Axial flux induction motor, design and evaluation of steady state modeling using equivalent circuit”, 2017 8th Power Electronics, Drive Systems & Technologies Conference (PEDSTC), pp. 353-358, DOI:10.1109/PEDSTC.2017.7910351, Mashhad, Iran (2017).

[14] Babu, VR., Soni, MP., and Manjeera, C. “Modeling of axial flux induction machine with sinusoidal winding distribution”, 2012 Annual IEEE India Conference (INDICON), pp. 481-486, DOI: 10.1109/INDCON.2012.6420666, Kochi, India (2012).

[15] Marousi Noushabadi, M., Javadi, S., Taghipour Boroujeni, S. “Design and modeling of an axial flux permanent magnet consequent pole machine”, Scientia Iranica, (), pp. -. doi: 10.24200/sci.2024.63574.8473, (2024).

[16] Wei, L., Han, Y., et al. “Investigation of a double-stator consequent-pole dual-PM machine for electric vehicle propulsion”, in IEEE Journal of Emerging and Selected Topics in Power Electronics, DOI: 10.1109/jestpe.2024.3472449 , (2024).

[17] Li, Z., Huang, X., et al. “An improved hybrid field model for calculating on-load performance of interior permanent-magnet motors”, IEEE Trans. Ind. Electron. **68**(10), pp. 9207–9217, DOI: 10.1109/TIE.2020.3029477, (2021).

[18] Faradonbeh, V.Z., Rahideh, A., et al. “Analytical modeling of slotted, surface mounted permanent magnet synchronous motors with different rotor frames and magnet shapes”, in IEEE Transactions on Magnetics, **57**(1), pp.1-13, Art no. 8100413, DOI: 10.1109/TMAG.2020.3032648, (2021).

[19] Liu, G., Jiang, S., et al. “ Modular reluctance network simulation of a linear permanent-magnet Vernier machine using new mesh generation methods”, IEEE Trans. Ind. Electron. **64**(7), pp. 5323–5332, DOI: 10.1109/TIE.2017.2677347, (2017).

[20] Faradonbeh, V.Z., Rahideh, A., “2-D analytical on-load electromagnetic model for double-layer slotted interior permanent magnet synchronous machines”, IET Electr. Power Appl, **16**(3), pp. 394-406, https://doi.org/10.1049/elp2.12162, March (2022).

[21] Faradonbeh, V.Z., Rahideh, A., Markadeh, G.A. "Analytical model for slotted stator brushless surface inset permanent magnet machines using virtual current theory", IET Electr. Power Appl. **14**(14), pp. 2750–2761, https://doi.org/10.1049/iet-epa.2020.0641, (2020).

[22] Pourahmadi-Nakhli, M., Rahideh, A., Mardaneh, M. “Analytical 2-D model of slotted brushless machines with cubic spoke-type permanent magnets”, IEEE Trans. Energy Convers. **33**(1), pp. 373–382, DOI: 10.1109/TEC.2017.2726537, (2018).

[23] Hajdinjak, M., Miljavec, D. “Analytical calculation of the magnetic field distribution in slot-less brushless machines with U-shaped interior permanent magnets”, IEEE Trans. Ind. Electron, **67**(8), pp. 6721–6731, DOI: 10.1109/TIE.2019.2939967, Aug (2020).

[24] Tang, C., et al. “Comparison of subdomain, complex permeance, and relative permeance models for a wide family of permanent-magnet machines”, in IEEE Transactions on Magnetics, **57**(2), pp.1-5, Art no. 8101205, DOI: 10.1109/TMAG.2020.3009416, (2021).

[25] Faradonbeh, V.Z., et al. “2-D analytical no-load electromagnetic model for slotted interior permanent magnet synchronous machines”, in IEEE Transactions on Energy Conversion, **36**(4), pp. 3118-3126, DOI: 10.1109/TEC.2021.3064034, Dec (2021).

[26] Jia, L., Lin, M., et al. "Modeling and analysis of axial flux permanent magnet machines with stator module misalignment", in IEEE Transactions on Applied Superconductivity, **34**(8), pp. 1-5, Art no. 5203605, DOI: 10.1109/TASC.2024.3420295, Nov (2024).

[27] Huang, R., Song, Z., et al. “An improved magnetic equivalent circuit method for segmented-halbach axial-flux permanent magnet machines”, in IEEE Transactions on Transportation Electrification, **9**(2), https://doi.org/10.1109/TTE.2022.3223960, June (2023).

[28] Wang, Q., Zhao, F., and Yang, K. “Analysis and optimization of the axial electromagnetic force for an axial-flux permanent magnet vernier machine”, in IEEE Transactions on Magnetics, **57**(2), pp. 1-5, Art no. 8100605, DOI: 10.1109/TMAG.2020.3005216, Feb (2021).

[29] Ma, c., An, Y., et al. “3-D Analytical model and direct measurement method of ultra-thin open-circuit air-gap field of interior permanent magnet synchronous motor with multi-segmented skew poles and multi-layered flat wire windings for electric vehicle”, in IEEE Transactions on Energy Conversion, **35**(3), pp. 1316-1326, DOI: 10.1109/TEC.2020.2982450, Sep (2020).

[30] Ghahfarokhi, M.M., Damaki, A., et al. “Analytical modelling and optimization of line start LSPM synchronous motors”, IET Electr. Power Appl, **14**(3), pp. 398-408, https://doi.org/10.1049/iet-epa.2019.0644, March (2020).

Figure:

Fig 1. Structure of the proposed model

Fig 2. Top view of the proposed model

Fig 3. Magnetic linkage and leakage flux path

Fig 4. Coils arrangement

Fig 5. Schematic of analytical model with linear structure

Fig 6. The structure of the slotted machine in the radius of 30 mm

Fig 7. The structure of the slot-less machine in the radius of 30 mm

Fig 8. The main MEC of the slot-less machine

Fig 9. The simplified MEC of the slot-less machine

Fig 10. The MEC of the slot-less machine without leakage reluctance

Fig 11. Equivalent circuit of machine with simplified structure

Fig 12. Flux passing path in the air gap function method

Fig 13. Flux passing path in the open area

Fig 14. Vertical flux density diagram in slot-less machine by analytical method

Fig 15. Vertical flux density diagram in slot-less machine

Fig 16. Flux path in slotted machine

Fig 17. Air gap length in slotted machine

Fig 18. Vertical flux density diagram in slotted machine by analytical method

Fig 19. Vertical flux density diagram in slotted machine

Table:

Table 1. Characteristics of consequent pole permanent magnet generator

Biographies

Mahmoud Marousi Noushabadi was born in Kashan, Iran, on 1989. He received a B.Sc. degree in electrical engineering from Technical and Vocational University, Kermanshah, Iran, in 2012 and an M.Sc. degree in electrical power engineering from Islamic Azad University, Kashan, Iran in 2016. He is currently a Ph.D. student in Electrical Power Engineering at Islamic Azad University, Kashan, Iran. His special fields of interest include designing, analyzing, and optimizing electric machines and hybrid vehicles.

Saeid Javadi was born in Aran and Bidgol, Iran, on March 21, 1969. He received the B.Sc. degree in communication engineering and the M.Sc. and Ph.D. degrees in electrical power engineering from Amirkabir University of Technology, Tehran, Iran, in 1992, 1999 and 2010, respectively. He is currently an Assistant Professor in the Department of Electrical and Computer Engineering, Kashan Branch, Islamic Azad University, Kashan, Iran. His special fields of interest include the design, analysis and optimization of electric machines and hybrid vehicles.

Samad Taghipour Boroujeni received the B.Sc., M.Sc., and Ph.D. degrees in electrical engineering from the Department of Electrical Engineering, Amirkabir University (Tehran Polytechnic), Tehran, Iran, in 2003, 2005, and 2009, respectively. In 2008, he was a Visiting Scholar with the Electrical Engineering Department, Padova University, Padova, Italy. In 2009, he joined the Department of Engineering, Shahrekord University, Shahrekord, Iran, as an Assistant Professor, where he was serving as an Associate Professor from 2016 to 2020. He had a postdoctoral carrier in 2018-2020 in Lorrain University, Nancy, France in GREEN Lab. He has been a Full Prof. since 2020 at Shahrekord University. His research interests include modeling, design, analysis, optimization, and control of electrical machines, especially variable-speed generators.

List of Figure:

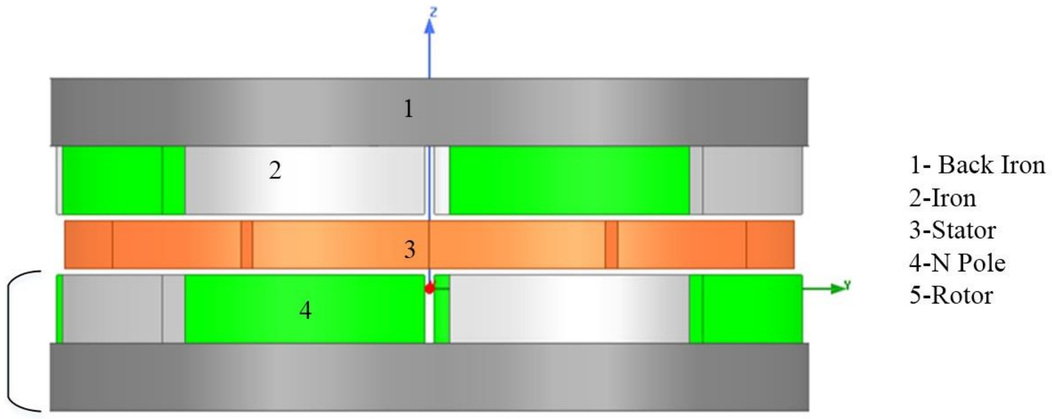

Fig 1. Structure of the proposed model

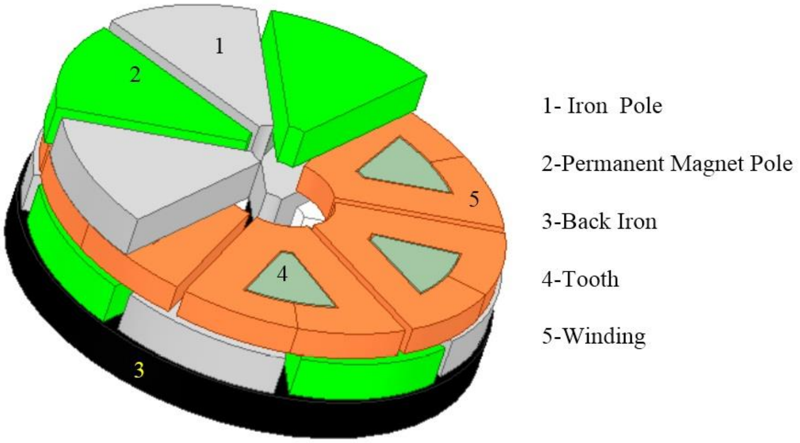
1
2
5
4
3
1- Iron Pole
2-Permanent Magnet Pole
3-Back Iron
4-Tooth
5-Winding

Fig 2. Top view of the proposed model

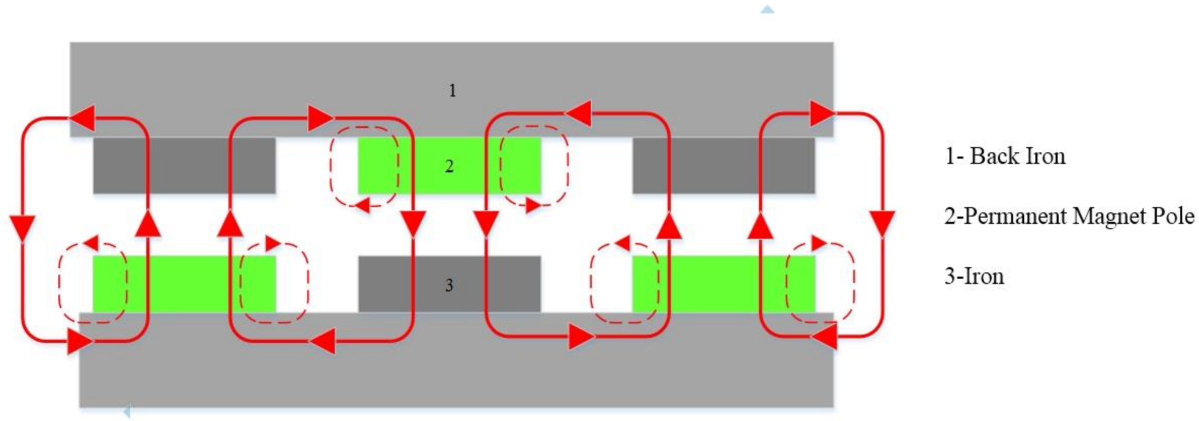
1
2
3
1- Back Iron
2-Permanent Magnet Pole
3-Iron

Fig 3. Magnetic linkage and leakage flux path

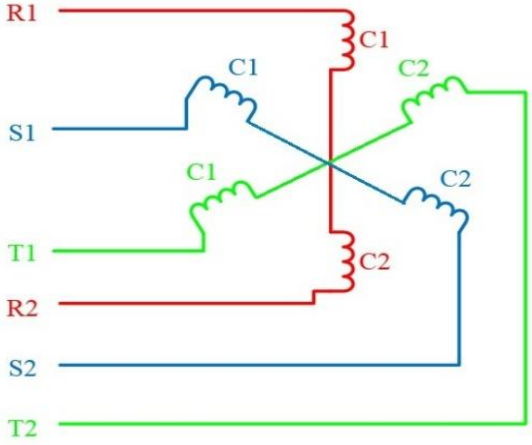
R1
C1
S1
C1
C2
C1
C2
T1
C2
R2
S2
T2

Fig 4. Coils arrangement

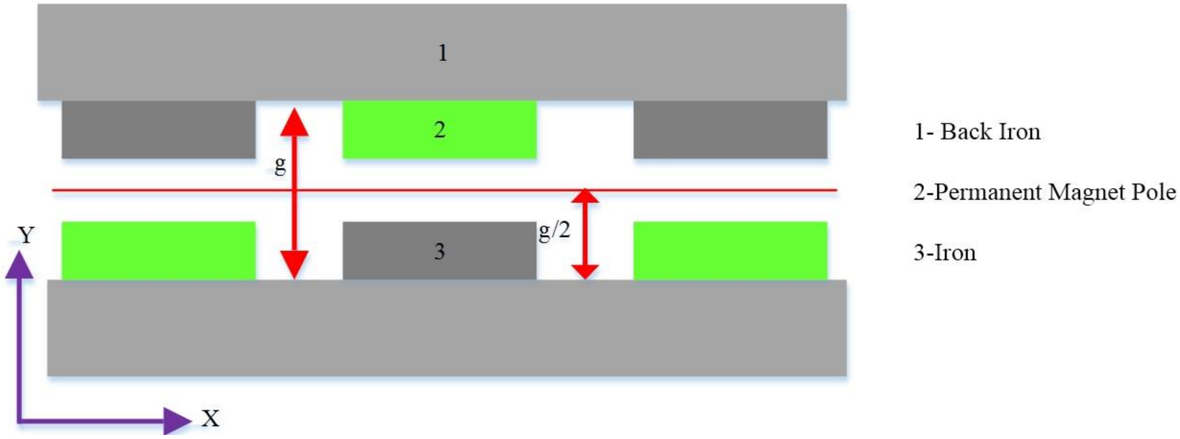
1
2
g
g/2
3
Y
X
1- Back Iron
2-Permanent Magnet Pole
3-Iron

Fig 5. Schematic of analytical model with linear structure

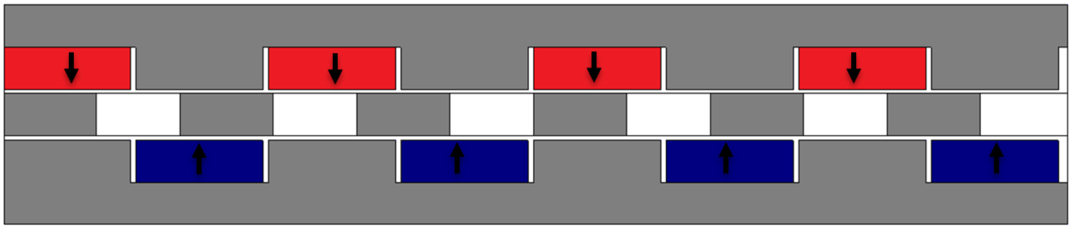

Fig 6. The structure of the slotted machine in the radius of 30 mm

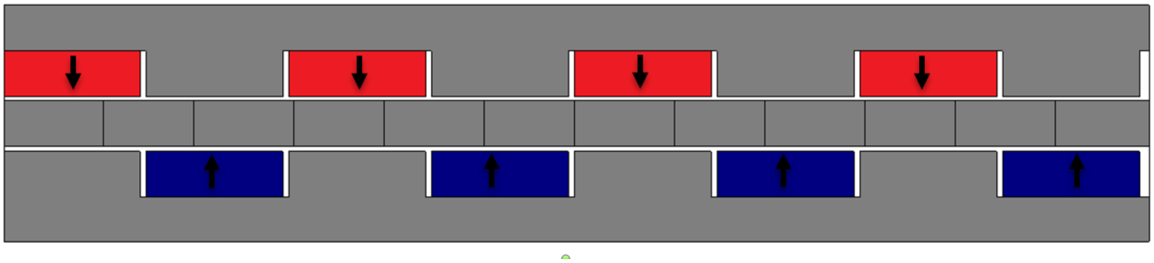

Fig 7. The structure of the slot-less machine in the radius of 30 mm

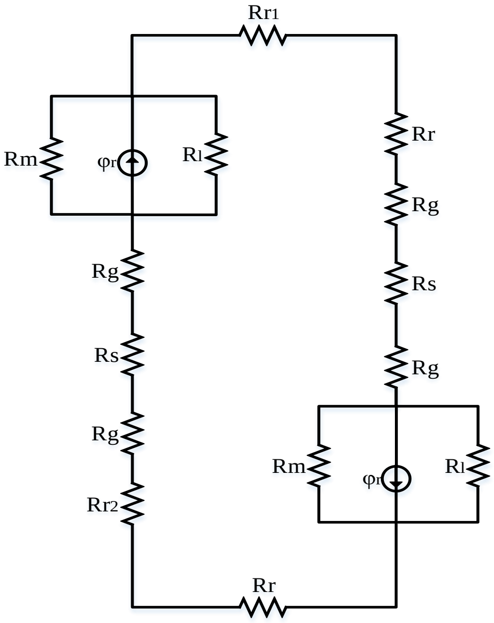
Rr1
Rm
φr
Rl
Rr
Rg
Rs
Rg
Rg
Rs
Rg
Rr2
Rm
φr
Rl
Rr

Fig 8. The main MEC of the slot-less machine

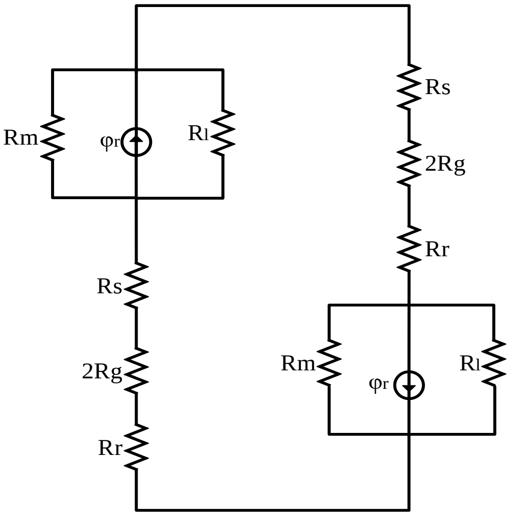
Rm
φr
Rl
Rs
2Rg
Rr
Rs
2Rg
Rr
Rm
φr
Rl

Fig 9. The simplified MEC of the slot-less machine

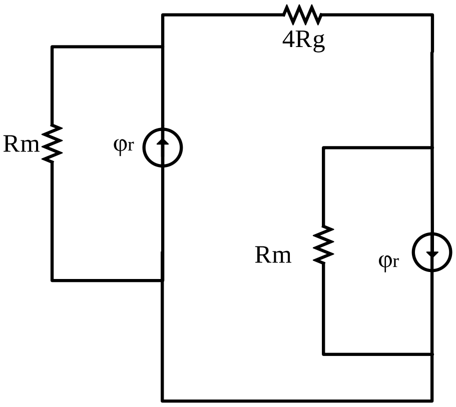

Fig 10. The MEC of the slot-less machine without leakage reluctance

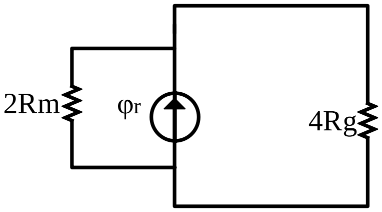

Fig 11. Equivalent circuit of machine with simplified structure

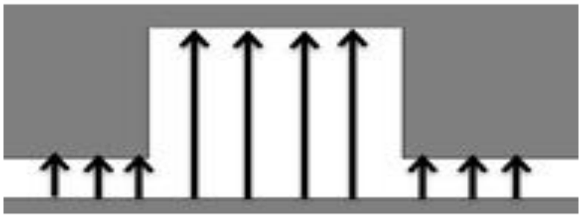

Fig 12. Flux passing path in the air gap function method

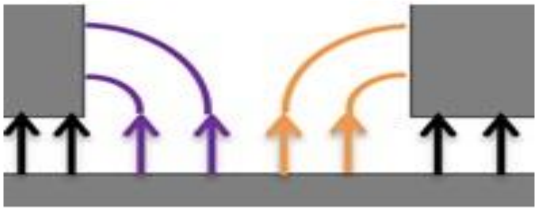

Fig 13. Flux passing path in the open area

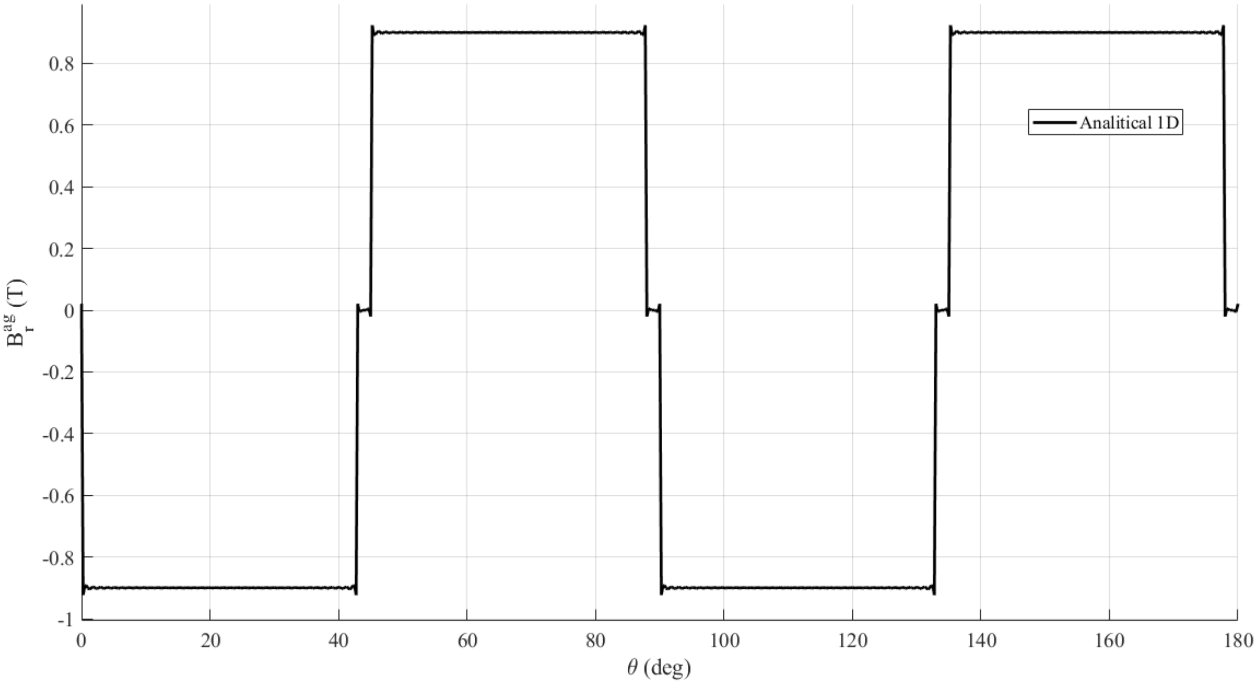

Fig 14. Vertical flux density diagram in slot-less machine by analytical method

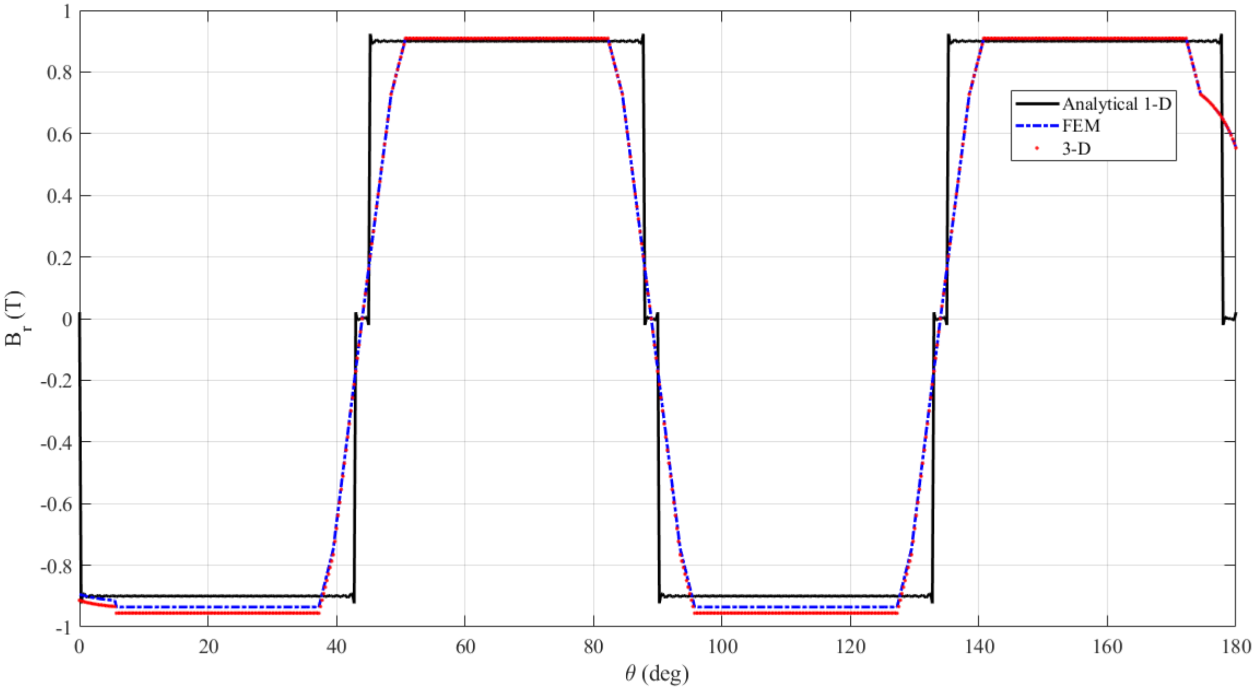

Fig 15. Vertical flux density diagram in slot-less machine

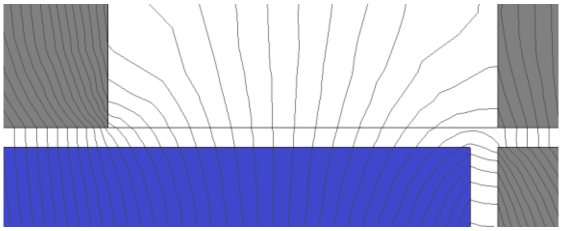

Fig 16. Flux path in slotted machine

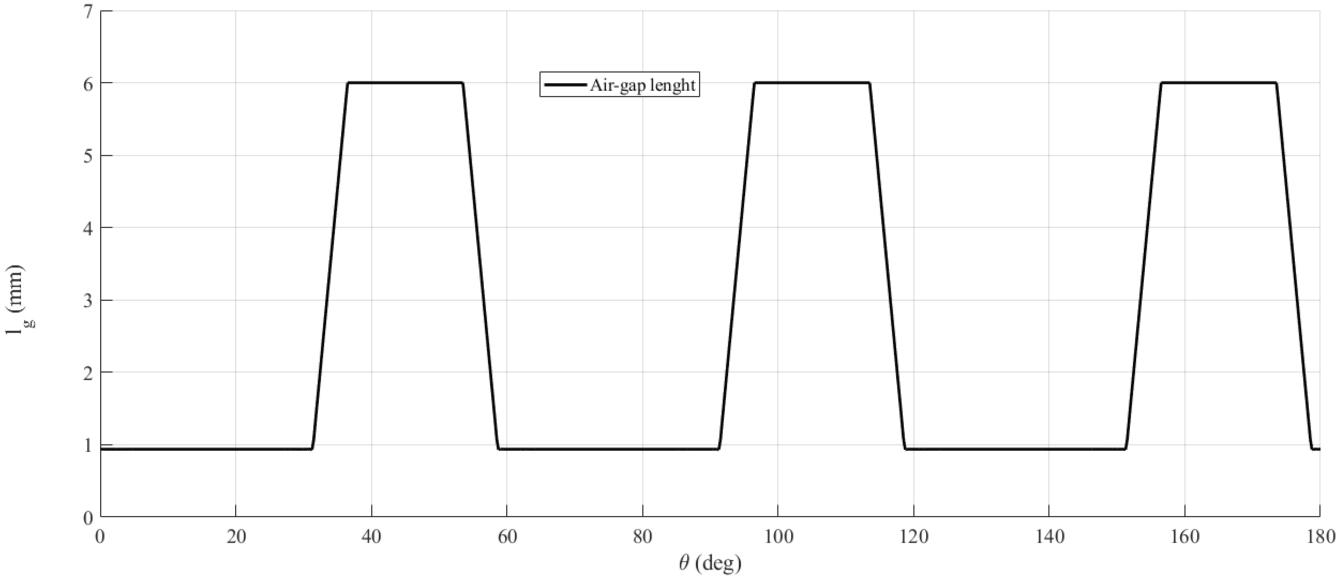

Fig 17. Air gap length in slotted machine

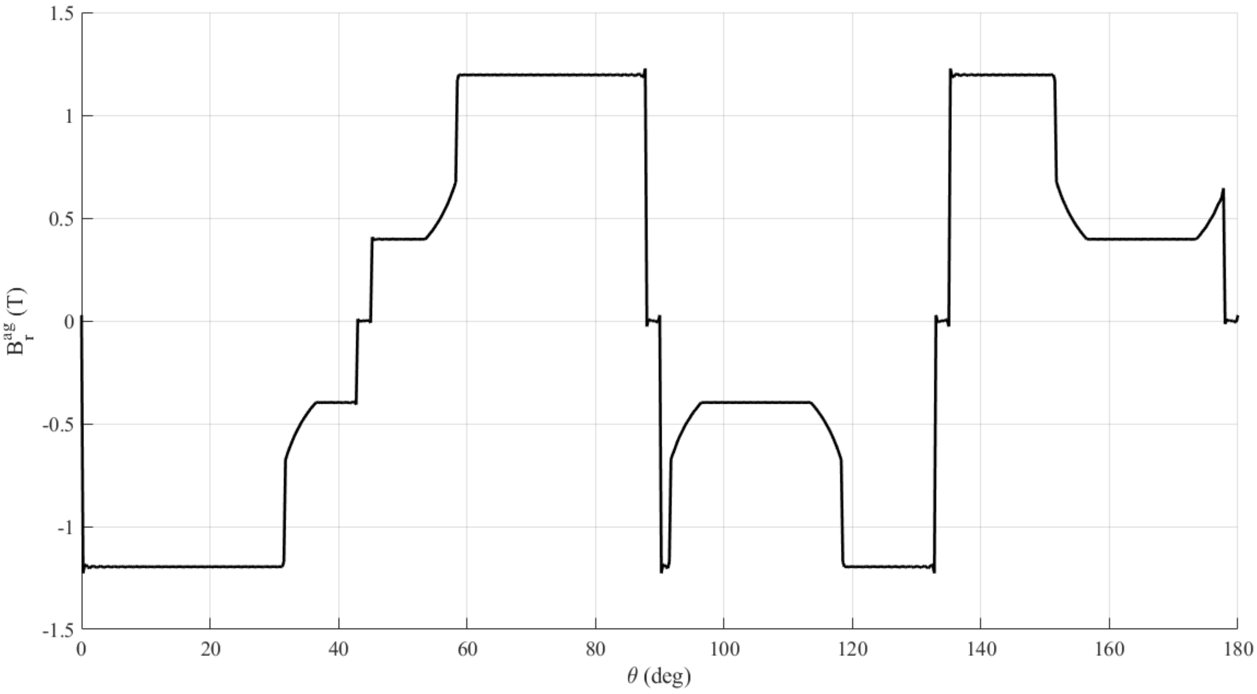

Fig 18. Vertical flux density diagram in slotted machine by analytical method

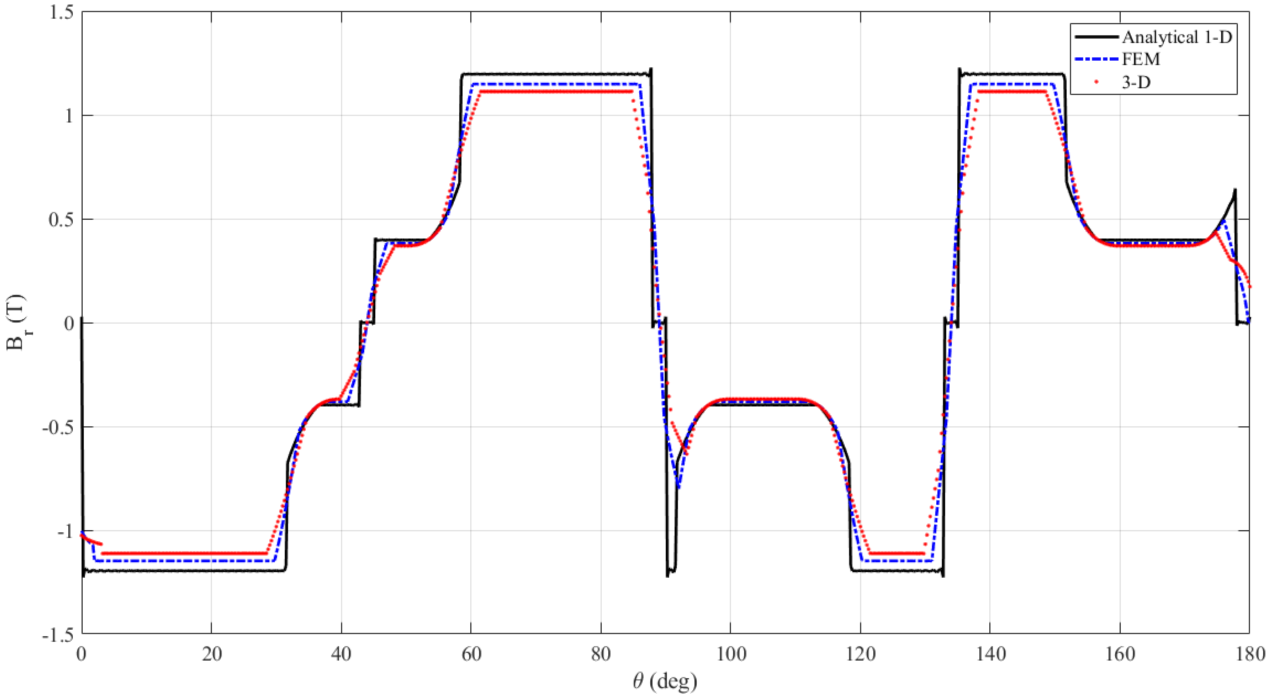

Fig 19. Vertical flux density diagram in slotted machine

List of table:

Table 1. Characteristics of consequent pole permanent magnet generator

Parameter	Values
Number Of Phases	3
Number Of Coils	6
N_{Coil}	60
$N_{S\ Phase}$	120
Wire Diameter	0.75 (mm)
Number Of Poles (NdFe35)	8
B_{rem} Residual Flux Density Of PM	1.2 (T)
Outer Radial Length Of PM	45 (mm)
Inner Radial Length Of PM	4 (mm)
Permanent Magnet Arc Angel	43°
Distance Between Poles	2°
Pole Thickness	10 (mm)
Thickness Of Back Iron	10 (mm)
Outer Radius Of Back Iron Disc	55 (mm)
Axial Length Of Generator	52 (mm)
Air Gap	1 (mm)
Outer Radial Length Of Coil (ro)	54.5 (mm)
Inner Radial Length Of Coil-1 (ri)	44.5 (mm)
Inner Radial Length Of Coil-2 (rii)	12 (mm)
Coil Width	10 (mm)
Coil Height	10 (mm)
Coil Arc Angele	57°
Tooth Length	19.75 (mm)
Tooth Width	2.5 (mm)
Tooth Arc Angele	54°

Speed	1000 (rpm)